Chinese Physics B

PAPER

Critical behavior and effect of Sr substitution in double perovskite Ca_2CrSbO_6*

Critical behavior and effect of Sr substitution in double perovskite Ca_2CrSbO_6*

Yuan-Yuan Jiao(焦媛媛)[1,2,3,†], Jian-Ping Sun(孙建平)[3], and Qi Cui(崔琦)[3,4]

[1] The State Key Laboratory of Refractories and Metallury, Wuhan University of Science and Technology, Wuhan 430081, China
[2] Faculty of Science, Wuhan University of Science and Technology, Wuhan 430062, China
[3] Beijing National Laboratory for Condensed Matter Physics and Institute of Physics, Chinese Academy of Sciences, Beijing 100190, China
[4] University of Chinese Academy of Sciences, Beijing 100049, China

(Received 1 July 2020; revised manuscript received 26 October 2020; accepted manuscript online 31 October 2020)

The double perovskite Ca_2CrSbO_6 exhibits a ferromagnetic long-range order below $T_c = 13$ K and a saturation magnetization of 2.35 μ_B at 2 K. In this study, the polycrystalline Ca_2CrSbO_6 is synthesized under high pressure and high temperature, and the critical behavior of the ferromagnetic material as well as the effects of the magnetic behavior due to the isovalent substitution of Sr^{2+} for Ca^{2+} is investigated. Also studied are the ferromagnetic criticality of the double perovskite Ca_2CrSbO_6 at the ferromagnetic transition temperature $T_c \approx 12.6$ K from the isotherms of magnetization $M(H)$ *via* an iteration process and the Kouvel–Fisher method. The critical exponents associated with the transition are determined as follows: $\beta = 0.322$, $\gamma = 1.241$, and $\delta = 4.84$. The magnetization data in the vicinity of T_c can be scaled into two universal curves in the plot of $M/|\varepsilon|^{\beta}$ *versus* $H/|\varepsilon|^{\beta+\gamma}$, where $\varepsilon = T/T_c - 1$. The obtained β and γ values are consistent with the predicted values from a three-dimensional Ising model. The effects of Sr substitution on the double perovskite Ca_2CrSbO_6 are taken into consideration. As the Sr content increases, the $(Ca_{2-x}Sr_x)CrSbO_6$ polycrystal shows a continuous switch from ferromagnetic to antiferromagnetic behavior.

Keywords: high-temperature and high-pressure synthesis, ferromagnet, Ca_2CrSbO_6

PACS: 75.10.–b, 75.50.Cc **DOI:** 10.1088/1674-1056/abc67b

1. Introduction

Due to their physical properties and technological applications, double perovskite oxides have been widely studied in recent decades.[1–4] Studies of the double perovskite Sr_2FeMoO_6 have been reported for its room temperature magnetoresistance (MR) and half-metallic conduction properties.[5,6] The general formula of a perovskite-derived double perovskite structure is $A_2BB'4O_6$ (A = divalent cation or rare-earth metal, and B = transition metal). The ideal double perovskites can be viewed as a regular arrangement of corner-sharing BO_6 and $B'O_6$ octahedra occupied by the large cations (A). The crystal structure of perovskites can be divided into cubic ($Fm3m$), tetragonal ($I4/m$) and monoclinic ($p2/n$) based on the size of A.[7]

Among the various double perovskite oxides, A_2CrSbO_6 (A = Ca, Sr) has received attention most due to their different magnetic structures. Retuerto *et al.* first synthesized the double perovskite Ca_2CrSbO_6 and reported its structure and magnetic properties.[8] The Ca_2CrSbO_6 shows a monoclinic structure [$a = 5.4932(3)$ Å, $b = 5.4081(3)$ Å, $c = 7.6901(5)$ Å, $\beta = 90.0022(1)$ Å, at 300 K], and belongs to the space group $P21/n$. The Cr and Sb cations are almost completely ordered in the B-sublattice of the perovskite structure. They reported that the Ca_2CrSbO_6 behaves as a Curie–Weiss paramagnet at high temperatures with $\mu_{eff} = 3.53(1)$ μ_B and $\theta_P = 8$ K. It exhibits a robust ferromagnetic component below the ordering temperature of $T_c = 13$ K, with a saturation magnetization of 2.36 μ_B/f.u. at 5 K. The electronic band structure and the ferromagnetic properties of the double perovskite Ca_2CrSbO_6, calculated by the first-principles method, were reported by Yi *et al.*[9] The Ca_2CrSbO_6 was found to have a stable ferromagnetic ground state, and the spin magnetic moment per molecule was calculated to be 2.99 μ_B. The contribution of chromium to the total magnetic moment was found to be the maximum. These results indicate that Ca_2CrSbO_6 is half-metallic, and it is the first example of a ferromagnetic double perovskite containing a non-magnetic B' cation. Thus, these materials can potentially serve as alternatives to other magneto resistive compounds. Hence, we are motivated to explore the critical behavior of Ca_2CrSbO_6 around T_c by analyzing the isotherms of magnetization $M(H)$ with an iteration process and the Kouvel–Fisher method.

A neutron diffraction investigation of Ca_2CrSbO_6 and Sr_2CrSbO_6 was reported by Alonso *et al.*[10] According to the neutron powder diffraction (NPD) data, each of the per-

*Project supported by the National Key Research and Development Program of China (Grant Nos. 2018YFA0305700 and 2018YFA0305800), the National Natural Science Foundation of China (Grant Nos. 11574377, 11888101, 11834016, 11874400, 11904272, and 11704292), and Jiao and Sun were sponsored by the China Postdoctoral Science Foundation and the Postdoctoral Innovative Talent Program.

†Corresponding author. E-mail: jiaoyuanyuan@wust.edu.cn

ovskites A_2CrSbO_6 (A = Ca, Sr) has a monoclinic crystal structure (space group $P21/n$). The Sr_2CrSbO_6 exhibits antiferromagnetic(AFM) long-range ordering below $T_N = 12$ K, whereas Ca_2CrSbO_6 has a ferromagnetic (FM) ordering below $T_c = 16$ K. Baidya and Saha-Dasgupta studied Sr_2CrSbO_6 and Ca_2CrSbO_6 by using the first-principles method to get an in-depth understanding of the switching from AFM to FM long-range order in Sr_2CrSbO_6, through replacing Sr by Ca.[11] They revealed that the first-neighbor magnetic interaction mediated by the super-exchange involving Sr/Ca dominates the second-neighbor magnetic interaction. It is the first nearest-neighbor interaction that governs its physical behavior. The differences in the hybridization effect between Sr and Cr from those between Ca and Cr, and the differences in the distortion of the crystal structure caused by the difference in size between Sr^{2+} and Ca^{2+} ions, bring about this interesting switching of magnetic properties at the Cr sublattice.

Previous studies have focused on the different magnetic properties of Ca_2CrSbO_6 and Sr_2CrSbO_6. There are a few experimental studies on the evolution of ferromagnetism of Ca_2CrSbO_6 into antiferromagnetism of Sr_2CrSbO_6. We successfully obtain the nearly single-phase Ca_2CrSbO_6 polycrystalline material by a solid-state reaction. The critical property associated with the ferromagnetic transition is characterized, and a comprehensive study on the responses of its magnetic behavior to the isovalent chemical substitution of Sr^{2+} for Ca^{2+} on the polycrystalline samples synthesized under high-pressure is performed.

2. Experimental details

Polycrystalline Ca_2CrSbO_6 samples were synthesized by solid-state reaction with appropriate stoichiometric amounts of $CaCO_3$ (99.99%), Cr_2O_3 (99.97%), and Sb_2O_5 (99.995%), which were heated in air at 800 °C for 12 h, and 1100 °C for 12 hours and subsequently at 1150 °C for 8 h. While the other components of $(Ca_{2-x}Sr_x)CrSbO_6$ ($x = 0.2$, 0.4, 1.0, 1.6, 1.8, 2.0) were obtained under high pressure and high temperature (HPHT) environment at 4 GPa and 1200 °C for 30 min. All HPHT syntheses in the present study were performed with a Kawai-type multianvil module.

Phase purities in the obtained $(Ca_{2-x}Sr_x)CrSbO_6$ ($x =$ 0.0, 0.2, 0.4, 1.0, 1.6, 1.8, 2.0) polycrystalline samples were first examined by powder x-ray diffraction (XRD) at room temperature with Cu $K\alpha$ radiation. The XRD data were analyzed with the Rietveld method by using the FULLPROF program. The direct current (DC) magnetic susceptibility was measured with a commercial magnetic property measurement system (MPMS-III, Quantum Design) in a temperature range of 2 K–300 K under an external magnetic field of $\mu_0 H = 0.1$ T. Isothermal magnetization $M(H)$ curves were recorded in a field range of −7 T to 7 T. The isothermal $M(H)$ curves of Ca_2CrSbO_6 were measured in a temperature range of 10 K–17 K, which covers the ferromagnetic transition.

3. Results and discussion

3.1. Critical behavior of Ca_2CrSbO_6

The temperature dependence of DC magnetic susceptibility $\chi(T)$ and its inverse $\chi^{-1}(T)$ measured under $\mu_0 H =$ 0.1 T in both zero-field-cooled (ZFC) and field-cooled (FC) mode are shown in Fig. 1(a). The ZFC curve and FC $\chi(T)$ curve overlap with each other, and the ferromagnetic transition around $T_c \approx 13$ K is visible from the sharp rise of $\chi(T)$ (Fig. 1(a)). The Curie–Weiss (CW) fitting to $\chi^{-1}(T)$ in a temperature range of 50 K–300 K is used in the paramagnetic region above T_c. The effective moment ($\mu_{eff} = 3.55\ \mu_B$) and the Weiss temperature ($\theta_{CW} = 18.7$ K) are extracted from the plots. The obtained μ_{eff} is close to the expected value of 3.87 μ_B for $S = 3/2$ of the spin-only paramagnetic Cr^{3+} ions. The positive θ_{CW} indicates the dominant ferromagnetic exchange interaction in the system. The $M(H)$ curve at 2 K exhibits a typical ferromagnetic behavior and reaches an expected saturation moment of 2.35 μ_B (Fig. 1(b)). These results are consistent with the previously reported data and confirm the high quality of the studied crystals.[10]

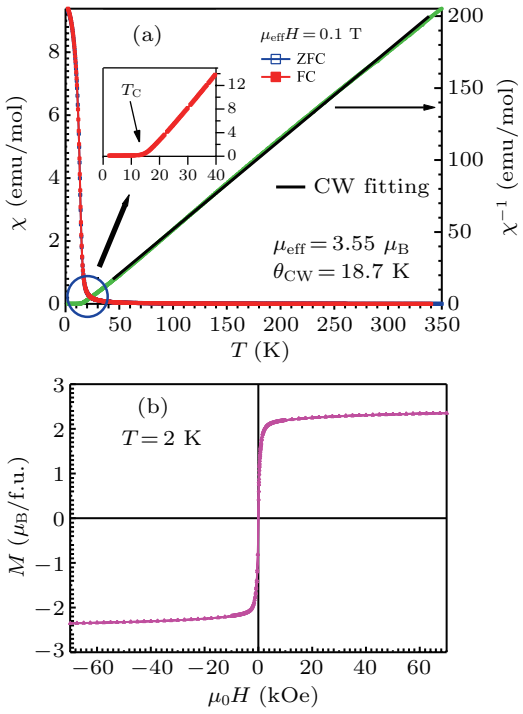

Fig. 1. (a) Temperature dependence of DC magnetic susceptibility $\chi(T)$ and its inverse $\chi^{-1}(T)$ measured in both zero-field-cooled (ZFC) mode and field-cooled (FC) mode under $\mu_0 H = 0.1$ T for Ca_2CrSbO_6, with solid line denoting Curie–Weiss (CW) fitting curve. (b) Isothermal magnetization $M(H)$ curve at 2 K for Ca_2CrSbO_6. The unit 1 Oe = 79.5775 A·m^{-1}.

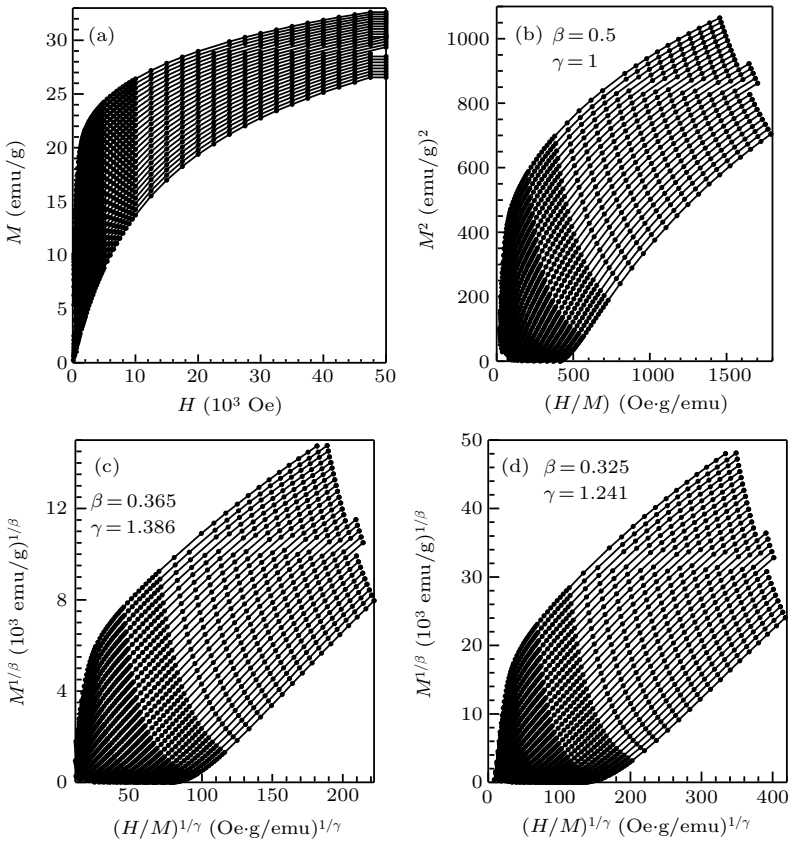

Fig. 2. (a) Isothermal magnetization curves between 10 K and 17 K, and the modified Arrott plots of these curves with critical exponents of (b) mean-field model $\beta = 0.5$, $\gamma = 1$, (c) 3D Heisenberg model $\beta = 0.365$, $\gamma = 1.386$, and (d) 3D Ising model $\beta = 0.325$, $\gamma = 1.241$.

Usually, a series of critical exponents, β, γ, and δ, which reflects the effective magnetic interactions. is used to characterize the critical behavior of compounds around the ferromagnetic phase transition.[12] Different critical exponents are derived theoretically for different models, *e.g.*, $\beta = 0.5$ and $\gamma = 1$ for the mean-field model, $\beta = 0.365$ and $\gamma = 1.386$ for the three-dimensional (3D) Heisenberg model, $\beta = 0.345$ and $\gamma = 1.316$ for the 3D *XY* model, and $\beta = 0.325$ and $\gamma = 1.24$ for the 3D Ising model.[13] These exponents are obtained by analyzing the isothermal magnetizations $M(H)$ near T_c, *viz.*,

$$M_s(T) \propto (T_c - T)^{\beta} \quad \text{for} \quad T < T_c, \tag{1}$$

$$\chi_0^{-1}(T) \propto (T - T_c)^{\gamma} \quad \text{for} \quad T > T_c, \tag{2}$$

$$M(H) \propto H^{1/\delta} \quad \text{for} \quad T = T_c, \tag{3}$$

where M_s is the spontaneous magnetization and χ_0^{-1} is the inverse initial magnetic susceptibility.

Figure 2(a) shows the isothermal magnetization curves, M *versus* H of Ca_2CrSbO_6 in a temperature range of 10 K–17 K, where the demagnetization effect is revised. These $M(H)$ data are replotted in the Arrott plot of M^2 *versus* H/M (Fig. 2(b)) and the modified Arrott plots of $M^{1/\beta}$ *versus* $(H/M)^{1/\gamma}$ with the critical exponents of the 3D Heisenberg model and the 3D Ising model (Figs. 2(c) and 2(d)). The Arrott plot (Fig. 2(b)) shows the possibility of a mean-field model, but the positive slope of the M^2 *versus* H/M confirms that the paramagnet–ferromagnet transition is continuous. The modified Arrott plots (Figs. 2(c) and 2(d)) show roughly parallel straight lines, which are difficult to distinguish intuitively alternative models to describe the ferromagnetism of Ca_2CrSbO_6 accurately.

To precisely determine the critical exponents, the magnetization is analyzed by using the general formulae (1)–(3).[12–14] Starting from the Arrott plot in Fig. 2(b), a third-order polynomial fit of the M^2 *versus* H/M curve is performed to obtain the first set of $M_s(T)$ and $\chi_0^{-1}(T)$ by extrapolating the corresponding fitting curves to the vertical and horizontal axis, respectively. The obtained $M_s(T)$ and $\chi_0^{-1}(T)$ are substituted into Eqs. (1) and (2) (Fig. 3(a)), to obtain the β and γ values, respectively. A modified Arrott plot of $M^{1/\beta}$ *versus* $(H/M)^{1/\gamma}$ is constructed by using the obtained data. Better critical exponent values for β and γ are obtained after the iterations converge.[15,16] The critical exponents converge to $\beta = 0.323$, $\gamma = 1.242$, and $T_c \approx 12.6$ K with three iterations (Fig. 3(a)). We check the Kouvel–Fisher (KF) relation,[17] *viz.*,

$$M_s(T)\,[\mathrm{d}M_s(T)/\mathrm{d}T]^{-1} = (T - T_c^-)/\beta, \tag{4}$$

$$\chi_0^{-1}(T)[\mathrm{d}\chi_0^{-1}(T)/\mathrm{d}T]^{-1} = (T - T_c^+)/\gamma. \tag{5}$$

A linear fit of the plot of $M_s(T)[\mathrm{d}M_s(T)/\mathrm{d}T]^{-1}$ and $\chi_0^{-1}(T)[\mathrm{d}\chi_0^{-1}(T)/\mathrm{d}T]^{-1}$ *versus* T yields $\beta = 0.322(8)$ and $\gamma = 1.241(9)$ (Fig. 3(b)). Both the values of β and γ obtained by the KF relation are quite consistent with the critical

isotherm $M(H)$ at T_c. The plot of M *versus* H of the isotherm at $T_c = 12.6$ K fits a line with $\delta = 4.84$ (Fig. 3(c)). Critical exponents of Ca_2CrSbO_6 obtained in this study satisfy the Widom scaling, $\delta = 1 + \gamma/\beta$.[17,18] The critical exponents, together with the theoretical values from different models are listed in Table 1 for comparisons.

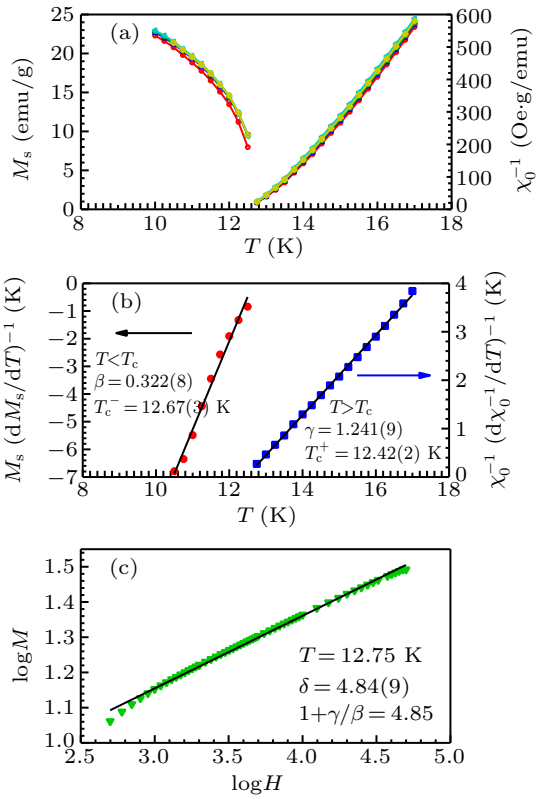

Fig. 3. Critical exponent β and γ, and critical temperatures T_c^- and T_c^+ determined from (a) iteration process started from mean-field Arrott plot, and (b) Kouvel–Fisher plots. (c) Critical isotherm at $T = 12.75$ K in double logarithmic plot and linear fitting to extract critical exponent δ, satisfying Widom scaling relation, $\delta = 1 + \gamma/\beta$.

To test the reliability of our analysis for the critical behavior in Ca_2CrSbO_6, isotherm is plotted based on the scaling hypothesis[13]

$$M(H,\varepsilon) = |\varepsilon|^{\beta} f_{\pm}(H/|\varepsilon|^{\beta+\gamma}), \tag{6}$$

where f^+ for $T > T_c$ and f^- for $T < T_c$ are regular analytical functions and $\varepsilon = T/T_c - 1$ is the reduced temperature. The $M/|\varepsilon|^{\beta}$ as a function of $H/|\varepsilon|^{\beta+\gamma}$ produces two universal curves: one is for $T < T_c$ and the other is for $T > T_c$ (Eq. (5)). The scaled data are obtained by using the values of β and γ obtained by the KF method and $T_c = 12.6$ K (Fig. 4); all the points indeed fall on the two curves. These well-scaled curves further confirm the reliability of the obtained critical exponents (Fig. 4).

In conclusion, the critical exponents associated with the transition for Ca_2CrSbO_6 are determined as follows: $\beta = 0.322$, $\gamma = 1.241$, and $\delta = 4.84$. The obtained β and γ values are consistent with the predicted values from the 3D Ising model. As is well known, the 3D Ising ferromagnet is rare in existing magnets since the spin degree of freedom is reduced. Moreover, a thorough study of specific heat is important for the critical behavior research. Therefore, a detailed specific heat study of Ca_2CrSbO_6 may be needed to further confirm the critical behavior of Ca_2CrSbO_6.

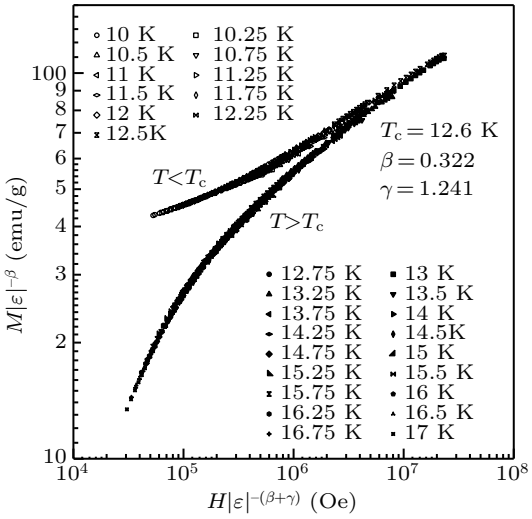

Fig. 4. Scaling plots for Ca_2CrSbO_6 below and above T_c based on critical temperature $T_c = 12.6$ K and $\beta = 0.322$, $\gamma = 1.241$.

Table 1. Critical exponents of Ca_2CrSbO_6 and theoretical values from three models.

	Ref.	β	γ	δ
Ca_2CrSbO_6	this work	0.322	1.241	4.84
Mean-field model	[13]	0.5	1.0	3.0
3D Heisenberg model	[13]	0.365	1.386	4.80
3D Ising model	[13]	0.325	1.241	4.82

3.2. Effect of Sr substitution in $(Ca_{2-x}Sr_x)CrSbO_6$

Previous studies have mainly focused on the synthesis of a pure phase and the theoretical study of electronic structures. Therefore, the present results may provide a new direction for the further study of Ca_2CrSbO_6. According to the neutron study of Ca_2CrSbO_6 and Sr_2CrSbO_6 by Retuerto *et al.*,[10] the crystal structures of Ca_2CrSbO_6 and Sr_2CrSbO_6 at room-temperature are all monoclinic (space group $P21/n$). These double perovskites exhibit different magnetic properties. The Ca_2CrSbO_6 exhibits long-range ferromagnetic order below $T_c = 16$ K and a saturation magnetization of 2.36 μ_B at 5 K, while Sr_2CrSbO_6 is an antiferromagnet material with a Neél temperature of 12 K and an ordered magnetic moment of 1.64(4) μ_B/Cr^{3+}. These magnetic effects motivate us to check the mechanism of evolution of the long-range ferromagnetic order of Ca_2CrSbO_6 into the antiferromagnetic property of Sr_2CrSbO_6 *via* the substitution of Sr^{2+} for Ca^{2+}. The polycrystalline Ca_2CrSbO_6 and Sr_2CrSbO_6 are synthesized by a solid-state reaction. The XRD patterns at room temperature (Fig. 5) are refined into a monoclinic structure ($P21/n$ space group). The crystal structure of Ca_2CrSbO_6 and Sr_2CrSbO_6 are displayed in Fig. 6. It should be noted that polycrystalline

Ca_2CrSbO_6 and Sr_2CrSbO_6 belong to the same crystal structure. The crystal structures of Ca_2CrSbO_6 and Sr_2CrSbO_6 projected onto the *a*–*b* plane are illustrated in Figs. 6(c) and 6(d), respectively. The Ca/Sr atoms sit in the hollow structure formed by the corner shared CrO_6 and SbO_6 octahedra. The Ca_2CrSbO_6 structure is found to be more distorted than the Sr_2CrSbO_6 which is driven by the smaller ionic radius of Ca^{2+} than that of Sr^{2+}. These results are consistent with the theoretical calculations by Baidya and Saha-Dasgupta.[11] In their reports, the average Cr–O–Sb angle of 180° is larger for Ca compound than for Sr compound. The average Cr–O bond length shows a small expansion for Ca compound compared with that for Sr compound.

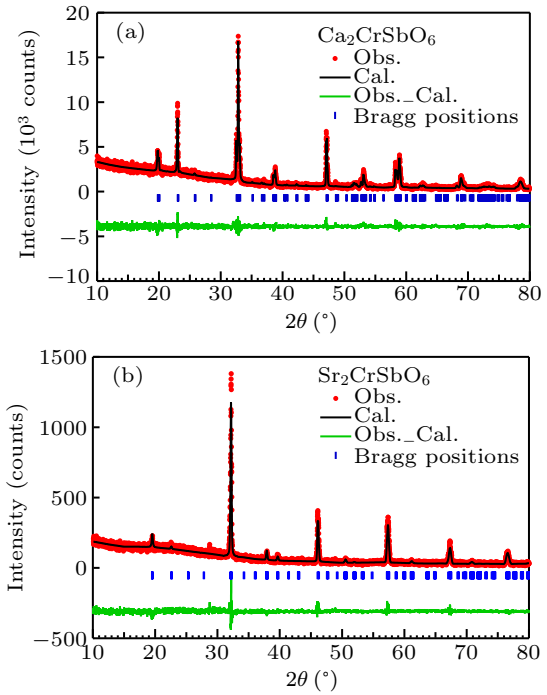

Fig. 5. The rietveld refinement on the XRD pattern of polycrystalline (a) Ca_2CrSbO_6 and (b) Sr_2CrSbO_6.

The average tilting angles of Ca_2CrSbO_6 and Sr_2CrSbO_6 are different. The average tilting angles are estimated at $\varphi = (180 - \theta)/2$ where $\theta = \langle Sb - O - Cr \rangle$;[10] for A = Ca, $\varphi = 13.5°$, whereas the tilting is much lower for A = Sr, where $\varphi = 5°$ accompanied with the larger tolerance factor. This result is consistent with the previously reported values.[8] We attempt to synthsize the $(Ca_{2-x}Sr_x)CrSbO_6$ solid solutions with varying Sr content by a solid-state reaction. However, the solid solutions cannot be obtained, for the melting point of mixture of Ca_2CrSbO_6 and Sr_2CrSbO_6 changes due to their mixing. After multiple attempts, $(Ca_{2-x}Sr_x)CrSbO_6$ ($x = 0.2$, 0.4, 1.0, 1.6, 1.8) solid solutions are obtained under high pressure and high temperature (HPHT) (4 GPa and 1200 °C for 30 min).

The powder x-ray diffraction patterns of a series of $(Ca_{2-x}Sr_x)CrSbO_6$ ($x = 0.0$, 0.2, 0.4, 1.0, 1.6, 1.8, 2.0), forming monoclinic structure are displayed (Fig. 7(a)). As expected, the lattice constant increases gradually with x increasing(Fig. 7(b)), due to the larger size of Sr^{2+}. It should be noted that the obtained $V(x)$ does not strictly follow a linear behavior or the Vegard's law. We believe that the deviation from Vegard's law in the series of $(Ca_{2-x}Sr_x)CrSbO_6$ is due to the different synthetic conditions between $x = 0.0$, 2.0, and $x = 0.2$–1.8.

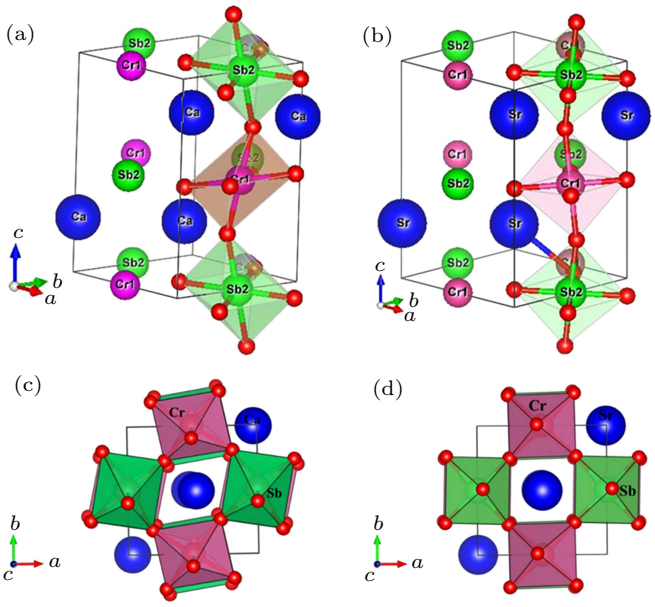

Fig. 6. Crystal structure of (a) Ca_2CrSbO_6 and (b) Sr_2CrSbO_6. Crystal structure of (c) Ca_2CrSbO_6 and (d) Sr_2CrSbO_6 projected onto *a*–*b* plane, respectively. The CrO_6 and SbO_6 octahedra are colored pink and green, respectively. The Ca/Sr atoms sit in hollow formed by corner shared CrO_6 and SbO_6 octahedra.

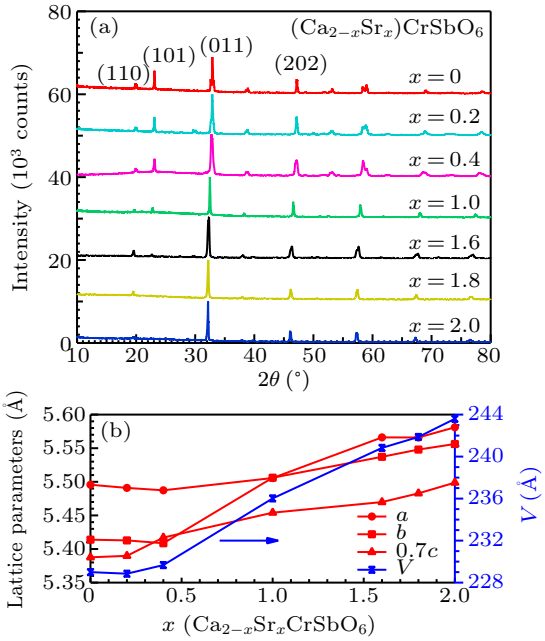

Fig. 7. (a) XRD pattern of polycrystalline $Ca_{2-x}Sr_xCrSbO_6$ ($x = 0.0$, 0.2, 0.4, 1.0, 1.6, 1.8, 2.0) and (b) unit-cell volume V *versus* Sr content x.

Figure 8 shows the magnetic susceptibility $\chi(T)$ for the series of $(Ca_{2-x}Sr_x)CrSbO_6$ under $\mu_0 H = 0.1$ T in both the ZFC mode and FC mode. When $x < 1.0$, with the increase in Sr content, the ferromagnetic transition temperature gradually moves toward lower temperature (Fig. 8(a)). When $x = 1.0$,

the ferromagnetic transition becomes inconspicuous. When $x > 1.0$, the ferromagnetic transition disappears and gradually changes into the antiferromagnetic transition. This is evident in $\chi^{-1}(T)$ curves (Fig. 8(b)). The inflection point T_N for $x = 0.18$ in the plot of χ^{-1} *versus* T is quite weak and is hard to define accurately. The broad peak in its derivative, $d\chi^{-1}/dT$, corresponds to the point where the curvature changes from convex to slight concave, and matches well to the $T_N \approx 8$ K in magnetic susceptibility. With the chemical substitution of Sr^{2+} for Ca^{2}, the structural distortions of Ca_2CrSbO_6 gradually diminish, and the magnetic transition gradually changes into antiferromagnetic transition as observed for Sr_2CrSbO_6.

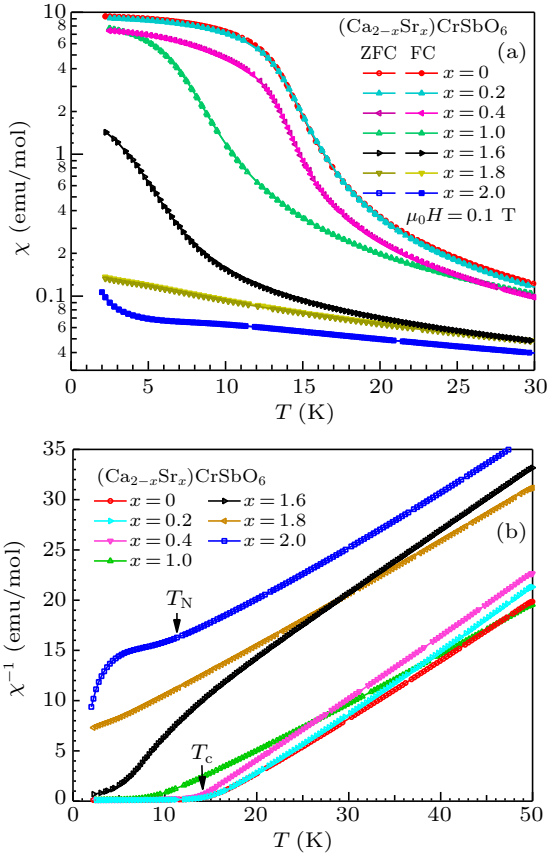

Fig. 8. Temperature dependence of (a) magnetic susceptibility $\chi(T)$ and (b) its inverse $\chi^{-1}(T)$ for the series of $Ca_{2-x}Sr_xCrSbO_6$ ($x = 0.0$, 0.2, 0.4, 1.0, 1.6, 1.8, 2.0) measured under $\mu_0 H = 0.1$ T in both zero-field-cooled (ZFC) and field-cooled (FC) modes.

Figure 9 shows the $M(H)$ curves for the series of $(Ca_{2-x}Sr_x)CrSbO_6$ under $T = 2$ K. A steep increase in $M(H)$ takes place between 0 and 1 T. The saturation magnetic moment approaches to ~ 2.35 μ_B in Ca_2CrSbO_6. With the increase in the Sr content, the saturation magnetic moment gradually decreases. When $x > 1.0$, the ferromagnetic transition disappears, and the magnetic reaction gradually changes into an antiferromagnetic transition, consistent with the results of the $\chi(T)$ curves. The T_c and T_N are obtained by fitting the $\chi(T)$ curves (Fig. 10). The ferromagnetic transition temperature T_c decreases with Sr varying in an x range of 0–1.0, and gradually converts into the antiferromagnetic transition. The antiferromagnetic transition temperature T_N increases with Sr content changing in an x range of 1.6–2.0. The results suggest that the continuous transition from ferromagnetism of Ca_2CrSbO_6 to antiferromagnetism of Sr_2CrSbO_6 is realized by doping different content of Sr in Ca_2CrSbO_6.

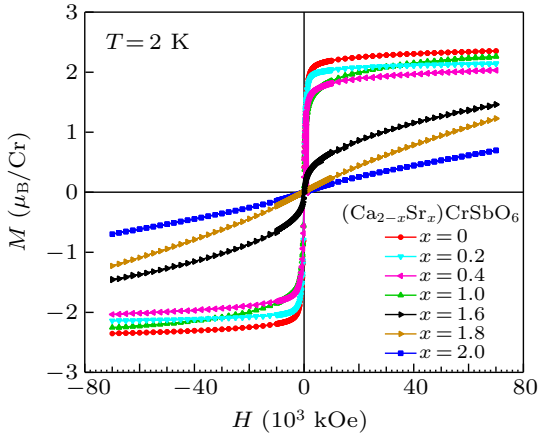

Fig. 9. Isothermal magnetization curves $M(H)$ for series $Ca_{2-x}Sr_xCrSbO_6$ ($x = 0.0$, 0.2, 0.4, 1.0, 1.6, 1.8, 2.0) between +7 T and −7 T at $T = 2$ K.

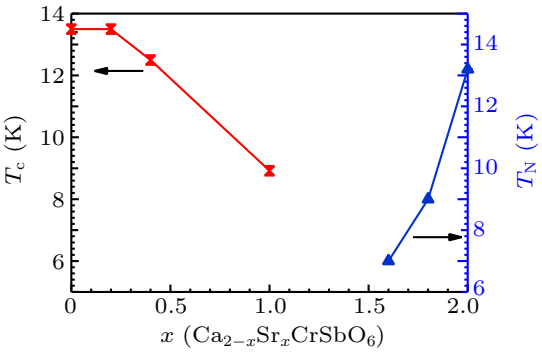

Fig. 10. T_c and T_N *versus* x for the series of $Ca_{2-x}Sr_xCrSbO_6$ ($x = 0.0$, 0.2, 0.4, 1.0, 1.6, 1.8, 2.0) obtained by fitting $\chi(T)$ curves.

According to the analysis by Alonso *et al.*,[10] changing the A cation in A_2CrSbO_6 (A = Sr, Ca) from Ca to Sr, causes structural distortions that can be responsible for the evolution from ferromagnetic to antiferromagnetic behavior. According to the Goodenough–Kanamori rules,[19] the direct super-exchange interaction *via* the half-occupied Cr:t_{2g} orbitals would be antiferromagnetic for an ideal Cr–O–Cr angle of 180°. Retuerto *et al.* speculated that the antiferromagnetism in Sr_2CrSbO_6 is because of the relatively weak, long-distance super-exchange interactions *via* the Cr–O–Sb–O–Cr path, thus the Neél temperature is relatively low.[10] The Cr–O–Sb–O–Cr pathways are antiferromagnetic provided that the Cr:t_{2g} orbitals are approximately co-planar (as in Sr_2CrSbO_6). If the CrO_6 octahedra are sufficiently twisted with respect to each other, then the ferromagnetic interactions arise as observed in Ca_2CrSbO_6.

Combined with our magnetic susceptibility results from $(Ca_{2-x}Sr_x)CrSbO_6$, the CrO_6 octahedra in Ca_2CrSbO_6 are sufficiently twisted with respect to each other and exhibit fer-

romagnetic interactions. We obtain the average tilting angle φ in $(Ca_{2-x}Sr_x)CrSbO_6$. For Ca_2CrSbO_6, $\varphi = 13.5°$; for $CaSrCrSbO_6$, $\varphi = 11.5°$; for Sr_2CrSbO_6, $\varphi = 5°$. The greater degree of octahedron tilting in Ca_2CrSbO_6 (the mean tilting angle $\varphi = 13.5°$) and Sr_2CrSbO_6 ($\varphi = 5°$) are consistent with the results reported by Retuerto *et al.*[10] With the chemical substitution of Sr^{2+} for Ca^{2+}, the average tilting angle graduallydecreases, the Cr:t_{2g} orbitals gradually become co-planar, and the super-exchange interactions in the Cr–O–Sb–O–Cr pathways gradually increase. With the increase in Sr content, the ferromagnetic interactions in Ca_2CrSbO_6 continuously convert into the antiferromagnetic interactions in Sr_2CrSbO_6. Our results showe a continuous magnetic transition between Ca_2CrSbO_6 and Sr_2CrSbO_6. Further theoretical investigations are needed to achieve a comprehensive understanding of the magnetic behavior in the $(Ca_{2-x}Sr_x)CrSbO_6$ systems.

4. Conclusions

In this work, we studied the ferromagnetic criticality of the double perovskite Ca_2CrSbO_6 at the ferromagnetic transition $T_c \approx 13$ K. A comprehensive study on the response of its magnetic evolution process to the isovalent chemical substitution of Sr^{2+} for Ca^{2+} in polycrystalline sample synthesized under high pressure is performed. Our results demonstrate that the critical exponents associated with the transition are determined as follows: $\beta = 0.322$, $\gamma = 1.241$, and $\delta = 4.84$. The magnetization data in the vicinity of T_c can be scaled into two universal curves in the plot of $M/|\varepsilon|^{\beta}$ *versus* $H/|\varepsilon|^{\beta+\gamma}$, where $\varepsilon = T/T_c - 1$. The obtained β and γ values are consistent with the predicted values of the 3D Ising model. With the increase in the content of Sr, the $(Ca_{2-x}Sr_x)CrSbO_6$ polycrystal continuously switches from ferromagnetism to antiferromagnetism. These results offer important experimental data for the ferromagnetic physical connotation study of Ca_2CrSbO_6. The present study will open a door for future investigating other perovskites.

Acknowledgment

We are grateful to Dr. Cheng J G for his help with the material preparation.

References

[1] Fresia E J, Katz L and Ward R 1959 *J. Am. Chem. Soc.* **81** 4783
[2] Longo J and Ward R 1961 *J. Am. Chem. Soc.* **83** 2816
[3] Galasso F and Pyle J 1963 *Inorg. Chem.* **2** 482
[4] Tomioka Y, Okuda T, Okimoto Y, Kumai R, Kobayashi K I and Tokura Y 2000 *Phys. Rev. B* **61** 422
[5] Kobayashi K I, Kimura T, Sawada H, Terakura K and Tokura Y 1998 *Nature* **395** 677
[6] Kim T H, Uehara M, Cheong S W and Lee S 1999 *Appl. Phys. Lett.* **74** 1737
[7] Ritter C, Ibarra M R, Morellon L, Blasco J, Garca J and Teresa J 2000 *J. Phys.: Condens. Matter* **12** 8295
[8] Retuerto M, Alonso J A, García-Hernández M and Martínez-Lope M J 2006 *Solid State Commun.* **139** 19
[9] Zhao Y, Ni G X, Liu H P and Yi L 2010 *Commun. Theor. Phys.* **53** 180
[10] Retuerto M, García-Hernández M, Martínez-Lope M J, Fernández-Díaz M T, Attfield J P and Alonso J A 2007 *J. Mater. Chem.* **17** 3555
[11] Baidya S and Saha-Dasgupta T 2012 *Phys. Rev. B* **86** 024440
[12] Mook A, Henk J and Mertig I 2017 *Phys. Rev. B* **95** 014418
[13] Stanley H E 1972 *Science* **176** 502
[14] Kaul S N 1985 *J. Magn. Magn. Mater.* **53** 5
[15] Yang F Y, Chien C L, Li X W, Gang X and Gupta A 2001 *Phys. Rev. B* **63** 092403
[16] Yanagihara H, Cheong W and Salamon M B 2002 *Phys. Rev. B* **65** 092411
[17] Kouvel J S and Fisher M E 1964 *Phys. Rev.* **136** A1626
[18] Cheng J G, Zhou J S, Goodenough J B, Su Y T and Sui Y 2011 *Phys. Rev. B* **83** 212403
[19] Goodenough J B 1955 *Phys. Rev.* **100** 564